Elucidating the Role of Electron Donating Groups in Halogen Bonding

Daniel P. Devore, Thomas L. Ellington, and Kevin L. Shuford*

Department of Chemistry and Biochemistry, Baylor University, One Bear Place #97348, Waco, TX 76798-7348, USA

E-mail: kevin_shuford@baylor.edu

Abstract

Computational quantum chemical techniques were utilized to systematically examine how electron donating groups affect the electronic and spectroscopic properties of halogen bond donors and their corresponding complexes. Unlike the majority of studies on halogen bonding, where electron withdrawing groups are utilized, this work investigates the influence of electron donating substituents within the halogen bond donors. Statistical analyses were performed on the descriptors of halogen bond donors in a prescribed set of archetype, halo-alkyne, halo-benzene, and halo-ethynyl benzene halogen bond systems. The σ-hole magnitude, binding and interaction energies, and the vibrational X$\cdots$N local force constant (where X = Cl, Br, I, and At) were found to correlate very well in a monotonic and linear manner with all other properties studied. In addition, enhanced halogen bonds were found when the systems contained electron donating groups that could form intramolecular hydrogen bonds with the electronegative belt of the halogen atom and adjacent linker features.

Introduction

Since the discovery of halogen bonds (XBs) in the 1800s,[1–4] significant advancements in the field have improved our understanding of halogen bond interactions in molecules, supramolecular structures, and biological systems. It has been reported throughout literature that the strongest XB interactions occur when the halogen bond donor contains strong electron withdrawing groups, a highly-polarizable halogen atom,[5–7] and significant *s*-character hybridization ($sp > sp^2 > sp^3$) of the atom covalently bonded to the principle halogen.[8–13] Such conditions generate an increased attraction between the halogen atom in the XB donor (Lewis acid) and the XB acceptor (Lewis base). This results from a noncovalent interaction between lone pairs on the acceptor and a depletion of electron density along the extension of the covalent bond between the halogen atom and the R-group (i.e., the σ-hole).[14–16]

While many studies focus on augmenting the σ-hole or halogen bond strength through stronger electron withdrawing substituents bonded to the R-group,[17–19] the polarizability of the halogen atom, or the hybridization of the R-group,[17,20,21] very few have examined other means to enhance halogen bonds. With the emergence of the hydrogen bond-enhanced halogen bonds (HBeXB),[22–24] there has been a new surge of research and development into the field of halogen bonding. In addition to σ-hole formation along the covalent bond axis, a belt-like region rich in electron density develops around the halogen. This electronegative region can behave as a Lewis base forming hydrogen bond (HB) or XB interactions. These additional interactions with the electronegative belt have been shown recently to enhance the strength of the XBs in complexes.[25–30]

In the work of Grabowski, the hydrogen and halogen bonds studied in $Cl^- \cdots HCCH$, $Cl^- \cdots ClCCH$, and $F^- \cdots ClCCH$ dimers were enhanced when the hydrogen bond donor (HF) was incorporated to form $Cl^- \cdots HCCH \cdots HF$, $Cl^- \cdots ClCCH \cdots HF$, and $F^- \cdots ClCCH \cdots HF$ trimers, respectively.[31] This demonstrates the possibility of cooperativity between multiple halogen and/or hydrogen bonds. Esrafili and Mohammadian-Sabet report a 12–24% enhancement in the $NH_4^+ \cdots NCX$ (X = F, Cl, and Br) hydrogen bond when the NCY (Y = H,

F, OH) molecule is noncovalently interacting with the X atom in NCX. They also find that the NCX$\cdots$NCY halogen bond is enhanced by 61–150% with the addition of NH_4^+.[32] These studies, amongst others,[33–37] show that significant enhancements are possible when multiple noncovalent interactions act in concert.

In addition to secondary interactions that enhance formation of stable XB complexes, another direction of study that will further our understanding of halogen bonds is the use of vastly different substituents. The effects that electron donating groups (EDGs) have on the σ-hole and the interaction strength in complexes is largely unknown. Are the XBs strengthened with the addition of EDGs bound to the R-group, or can we tune the strength of these halogen bonds for more specific applications? Does the positioning and strength of the EDG in the XB donor have any significant impact on the formation of the σ-hole and the noncovalent interactions that may occur? These questions motivated our present study to better understand the role that EDGs, coupled with secondary interactions, have on halogen bonding. Indeed, we show that the magnitude of the σ-hole and the interaction strength of the XB complexes vary with the position and orientation of the EDGs in the donors, and such quantities correlate very well with the properties that are most considered when studying these noncovalent interactions (e.g., $V_{S,max}$, E_{bind}, charge transfer in the complex, R–X bond length and force constant to name a few). The XB donors (Figure 1) and an ammonia acceptor are used to investigate the effects that the EDGs have on these interactions. Also taken into account is the size of the XB donor, the hybridization of the R-group, and the number, position, and orientation of EDG ring substituents in the XB donor. The halo-benzene and halo-ethynyl benzene XB donors with an EDG *ortho* to the principle halogen atom, and with the hydrogen atom in the EDG pointing toward the halogen, are shown to exhibit some of the most positive σ-holes and strongest interactions in the XB complexes. These results suggest that intramolecular hydrogen bond donors incorporated into the XB donor may offer some additional enhancement to halogen-bonded supramolecular structures.

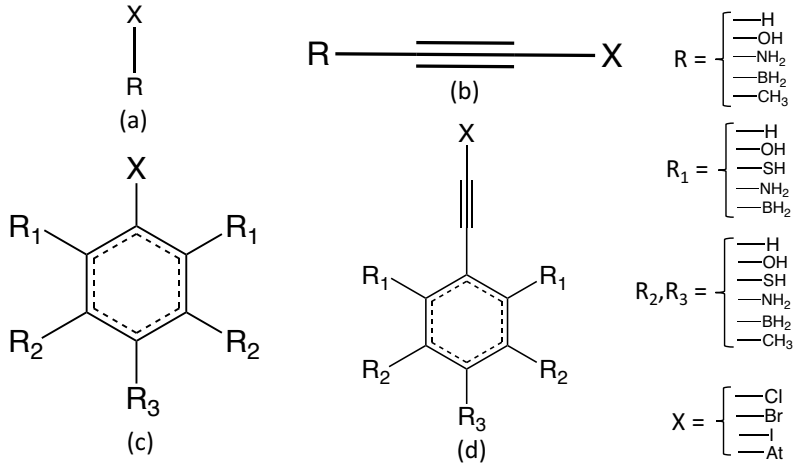

Figure 1: Schematic representation of the XB donors: (a) halo-archetypes (b) halo-alkynes, (c) halo-benzenes, and (d) halo-ethynyl benzenes.

Computational Details

Full geometry optimizations, harmonic vibrational frequency computations, and natural bond orbital (NBO) analyses[38–44] were performed on all XB donors and the corresponding XB complexes with ammonia as the acceptor. The calculations used the global hybrid M06-2X density functional,[45] in conjunction with a double-ζ quality correlation consistent polarized valence basis set augmented with diffuse functions on all atoms[46–48] with a relativistic pseudo-potential on bromine, iodine, and astatine centers (i.e., aug-cc-pVDZ for period 1–3 atoms; aug-cc-pVDZ-PP for Br, I, and At).[49,50] The selected level of theory is based on the extensive calibrations conducted by Kozuch and Martin.[51] The binding energy of the complex (E_{bind}) is calculated as the energy difference between the optimized geometries of the XB complex and the individual donor/acceptor molecules (i.e., $E_{bind} = E^{complex} - (E^{donor} + E^{acceptor})$). Vibrational frequency calculations were used to ensure that each structure was a minima (i.e., $n_i = 0$) on the M06-2X/aVDZ-PP potential energy surface. Boys-Bernardi counterpoise corrections were applied to account for basis set superposition error (BSSE).[52] Further characterization of bond and interaction strengths for the C–X, C≡C, X$\cdots$N, and where applicable the H$\cdots$X interaction, was determined through

local mode analysis (LMA). This is accomplished through decoupling the normal vibrational modes into their local stretching mode counterparts. Following the Badger rule,[53] a direct correlation between the local force constants obtained through LMA and the strength of the intra- and intermolecular interactions can be made. Further description of LMA can be found in the literature authored by Kraka et al.[54] The difference between the $R_{X\cdots N}$ bond length and the sum of the halogen's and nitrogen's van der Waals radii was used as a descriptor for the comparison of the length of the halogen bonding interactions.[55]

All geometry optimizations, harmonic vibrational frequency computations, NBO analyses, and where applicable, the gradients and Hessians therein, were performed using the Gaussian 16 software package.[56] All computations, unless otherwise stated (see Supporting Information (SI)), were performed using a pruned numerical integration grid composed of 175 radial shells (250 radial shells for second and higher period elements) and 974 angular points per shell along with a threshold of $< 10^{-9}$ for the RMS change in the density matrix during the self-consistent field procedure. The threshold for removing linear dependent basis functions was tightened from 10^{-6} to 10^{-7}. All electronic energies have been converged to at least 10^{-9} E_h, while the Cartesian forces of the gradient did not exceed 10^{-5} $E_h a_0^{-1}$. Pure angular momentum (i.e., $5d$, $7f$, etc.) basis functions were used instead of their Cartesian counterparts (i.e., $6d$, $10f$, etc.). The Multiwfn program[57] was utilized to identify the topology of the electron density of the molecules via the QTAIM method[58–60] and evaluate the electrostatic potential (ESP) surfaces using a total electron isodensity of 0.001 electrons/Bohr^3. Generation of all ESP maps was produced through Tachyon ray tracing libraries[61] available in the Visual Molecular Dynamics visualization software.[62] The local mode force constants and dipoles for each XB donor and corresponding XB complex were obtained utilizing the LModeA code developed by Kraka and co-workers.[54,63–65] Data analysis was performed through the pandas python package[66,67] with each correlation heat map, pair plot, and scatter plot produced through the seaborn and matplotlib python libraries.[68,69]

Results and Discussion

A thorough statistical analysis was performed for all XB systems in this study. Table 1 provides a detailed list and definition for all the properties that will be discussed. The heat maps presented in the main article display the Spearman rank correlations between parameters, while the analogous Pearson correlations can be found in the SI. These heat maps are partitioned according to the general parameter categories, where the energetic and spectroscopic parameters are displayed on the left hand side of the figures, and the structural and spectroscopic parameters are displayed on the right. Spearman correlations (denoted as rs) show how well a monotonic function can describe the relationship between two variables rather than the overall spread of the data. Pearson correlations (denoted as r), on the other hand, describe how linear the relationship between two variables is. Therefore, a positive Spearman (Pearson) correlation means that the relationship of the two variables is monotonically (linearly) increasing, whereas a negative value depicts the relationship as decreasing in a monotonic (linear) fashion. For reference, a strong monotonic and linear correlation is taken as $|rs| > 0.9$ and $|r| > 0.9$. The relationship between two variables has no correlation when $rs = 0$ and/or $r = 0$. The Spearman correlation is better suited to describe exponential and step functions, which can give a more inclusive description of the relationship between variables. Therefore, we opted to display the Spearman correlations in the heat maps throughout this article. Pearson correlations, however, still provide a valid and helpful account of the relationship between two variables, and those heat maps are provided in the SI. In addition, heat maps containing the absolute values of the correlations, for conspicuous determination of strong versus weak, are provided in the SI.

Table 1: Energetic, structural, and spectroscopic properties used in the statistical analyses.

Symbol	Definition
$V_{S,max}$	Magnitude of the σ-hole.
$\mathrm{V}_{max}(r)$	Depth or distance of the σ-hole, computed as the distance between the $V_{S,max}$ critical point and the geometric center of the halogen atom.
E_{bind}	Binding energy of the complex, calculated by taking the difference of the relaxed complex and the sum of relaxed monomers.
E_{int}	Interaction energy of the complex, calculated by taking the difference of the relaxed complex and the sum of the monomers in the complex geometry.
E_{bind}^{CP}	Counterpoise corrected binding energy of the complex.
E_{int}^{CP}	Counterpoise corrected interaction energy of the complex.
E_{donor}^{def}	Deformation energy of the XB donor.
$\mathrm{E}_{NH_3}^{def}$	Deformation energy of the NH_3 acceptor.
E(2)	Stabilization energy upon partial transfer of nitrogen lone pair electrons in the ammonia acceptor to the σ^* orbital of the C–X bond in the XB donor.
$\Delta\rho$	Magnitude of charge transferred from the XB acceptor to the XB donor.
$k_{X\cdots N}^{a}$	X$\cdots$N bond local force constant.
Δk_{C-X}^{a}	Change in the C–X bond local force constant upon complexation.
$\Delta k_{C\equiv C}^{a}$	Change in the C$\equiv$C bond local force constant upon complexation.
$\mathrm{R}_{X\cdots N}$	X$\cdots$N bond length.
$\Delta\mathrm{R}_{C-X}$	Change in the C–X bond length upon complexation.
$\Delta\mathrm{R}_{C\equiv C}$	Change in the C$\equiv$C bond length upon complexation.
$\mu_{X\cdots N}$	X$\cdots$N bond local dipole moment.
$\mu_{C-X}^{Complex}$	C–X bond local dipole moment in the XB complex.
μ_{C-X}^{Donor}	C–X bond local dipole moment in the XB donor.
$\mu_{C\equiv C}^{Complex}$	C$\equiv$C bond local dipole moment in the XB complex.
$\mu_{C\equiv C}^{Donor}$	C$\equiv$C bond local dipole moment in the XB donor.

Archetype Systems

To gain a better understanding of how electron donating groups affect the size and magnitude of the σ-hole, as well as the interaction strength upon complexation, we systematically examined an array of archetypal systems with an EDG present in the XB donor. These archetypal systems are of the form XR, where X is a halogen atom (Cl, Br, I, At) and R is an EDG (–H, –OH, $–NH_2$, $–BH_2$, $–CH_3$). Figure 2 shows the qualitative trends between the energetic, structural, and spectroscopic properties of the archetypal XB donors and

the corresponding complex with ammonia by using Spearman correlation. For the small polyatomic systems, the σ-hole depth or σ-hole distance ($V_{max}(r)$), defined as the distance of the critical point that represents the $V_{S,max}$ from the nuclear center of the halogen atom, does not have a very monotonic relationship with any other property, as indicated by low magnitude correlation values (left panel, 2nd column). The analogous heat map based on Pearson correlation (Figure S1, 2nd column) shows $V_{max}(r)$ also does not have a very linear relationship with the other properties. $V_{S,max}$, on the other hand, has a monotonic and relatively linear relationship with almost every other property related to halogen bonding (Figs. 2 and S1, first column of both panels). The only exception is the donor C–X dipole moment (μ_{C-X}^{Donor}), where C represents the atom bonded to the halogen (not necessarily a carbon atom). This likely results from the varying direction of the dipole moment, which depends on the electronegativity of the R group and the halogen atom. Note, some of the trends have a negative correlation that is due to the sign of the values $V_{S,max}$ is correlated to. For example, the correlation between $V_{S,max}$ vs. E_{bind} is monotonically negative because the sign of E_{bind} is negative. However, based on the very negative rank Spearman correlation ($rs = -0.97$), we can see that as $V_{S,max}$ becomes more positive, E_{bind} becomes more negative and therefore is inversely proportional. Physically, the more positive the $V_{S,max}$, the stronger the attraction of the XB donor to the Lewis base (i.e., ammonia), which correlates very nicely to the monomers binding more strongly to each other. This trend with $V_{S,max}$ vs. E_{bind} applies to the other energetic values associated with the interacting XB complex (i.e., E_{int}, E_{int}^{CP}, and E_{bind}^{CP}; where CP indicates counterpoise corrected) as well as the magnitude of charge transfer ($\Delta\rho$). $\Delta\rho$ is reported as a negative value, indicating that the charge is being transferred from the XB acceptor (Lewis base) to the XB donor (Lewis acid). Hence, the correlation of $V_{S,max}$ vs. $\Delta\rho$ is negative ($rs = -0.86$), showing that as the attractiveness of the halogen increases, the degree of electron density that is able to transfer across the halogen bond increases.

Additional insight can be gleaned by examining the distribution of data in the prop-

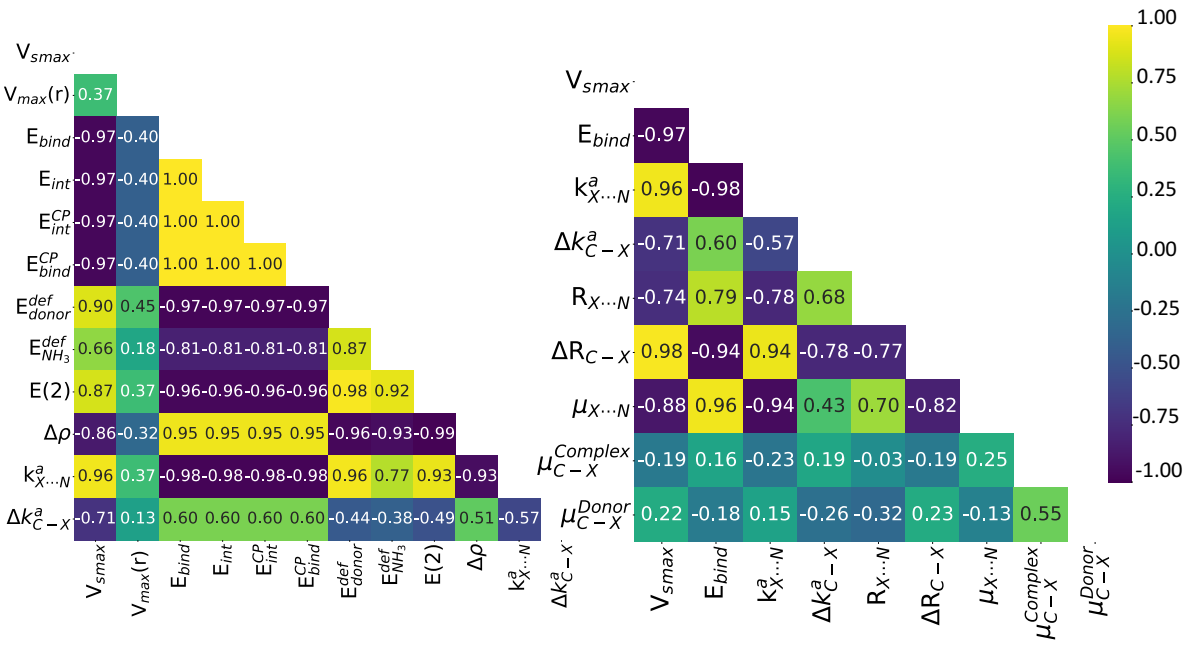

Figure 2: Spearman correlation heat map of the electronic and spectroscopic properties (left) and structural and spectroscopic properties (right) for the 13 archetype XB donors and corresponding complexes.

erties being studied for different donors. For example, the σ-hole data for astatine and iodine archetypes has a wide spread when considering the different $V_{S,max}$ values against every property (see distributions in Figure S5, top of 1st column). This is due to the large range of $V_{S,max}$ values that these two halogen atoms can accommodate when incorporated into XB donors, which allows for astatine and iodine containing complexes to form more easily. Bromine and especially chlorine, on the other hand, have narrow density plots. This illustrates that the inherent polarizability of the halogen atom is a very important factor to consider when designing XB donors, agreeing with previous findings on polarizability of halogen atoms.[5–7] Another insightful result can be attained by examining the pair distribution data for the different levels of theory. Figure S5 (columns 3-6) shows very similar distributions are obtained for the binding as well as interaction energies both with and without counterpoise corrections, indicating that BSSE is virtually negligible even with the smaller aVDZ(-PP) basis set. The density for chlorine archetypes is concentrated on the right (more

positive) side in a much more narrow distribution compared to the other halogen atoms. This shows that the chlorine-containing donors form much weaker noncovalent interactions in a narrow range of values due to the limited redistribution of electron density around the chlorine atom resulting from its small size and low polarizability. Due to the narrow range of binding and interaction energies seen from the density distribution curves and the strong monotonic and linear correlations that the binding and interaction energies have with the magnitude of charge transfer ($rs = 0.95$, $r = 0.97$), we can conclude that there is very little charge transfer from the ammonia acceptor to the chlorine containing XB donor. The binding and interaction energy distributions for iodine and astatine (and bromine to a lesser extent) are much broader (Figure S5, columns 3-6), showcasing the wide array of binding energies that the larger halogen atoms cover and their ability to form much stronger interactions.

Aligning with the correlations in Figures 2 and S1, the amount of charge transfer and the strength of the X$\cdots$N bond increase with more negative binding and interaction energies (left panel, rows 9 and 10 of column 3 in Figs. 2 and S1). These trends also follow chemical intuition, where as the interaction energy becomes increasingly more negative, the electron acceptor has a stronger "hold" on the electrons being donated by the Lewis base. This stronger propensity to retain electrons then translates to a stronger bond, which is represented by the local X$\cdots$N force constant ($k^a_{X\cdots N}$). The electrons transferred from the Lewis base (ammonia) being "pulled on" more strongly by the Lewis acid (XB donor) thus results in a more positive energy for electron transfer, represented as the second order perturbation NBO energy (E(2)). This can be seen from the negative correlation of charge transfer as well as binding and interaction energies vs. E(2) in Figure 2 ($rs = -0.99$, -0.96, and -0.96, respectively). This trend states that as the amount of electrons transferred (binding/interaction energy) increases (becomes more negative), the second order perturbation NBO energy for the partial transfer of the N lone pair to the σ^* orbital of the C–X bond in the XB donor becomes more positive.

A slightly different trend is observed for the deformation energies of the monomer units.

The deformation energy of the XB donor (E^{def}_{donor}) tends to have a very linear (Figure S1, 6th row and 7th column in left panel), monotonic (Figure 2, 6th row and 7th column in left panel) relationship with every other electronic and spectroscopic property being measured, barring the σ-hole distance and change in the C–X bond local force constant (Δk^a_{C-X}). These trends are understandable because the deformation energy represents the degree of change in the electronic structure that the XB donor undergoes from the ground state configuration upon complexation. This deformation occurs due to the XB donor donating and receiving electrons from the XB acceptor. The larger the degree of deformation (higher energy) in the XB donor, the stronger the XB donor "pulls" on the XB acceptor, thus increasing the amount of charge transfer and binding/interaction energy of the complex. The deformation energy of the acceptor (ammonia), on the contrary, does not have as monotonic or linear of a relationship with the other properties as the deformation energy of the XB donor. The reason for the ammonia deformation energy being less correlated to the other properties when compared to the XB donor deformation energy is because the electronic structure of ammonia does not change nearly as much as the XB donor upon complexation. While the lone pair on the nitrogen atom is interacting with the XB donor, there is little disturbance to the ammonia molecule. Hence, the deformation energy of the ammonia acceptor is limited.

Shifting to more of the structural and spectroscopic values, the X$\cdots$N bond length ($R_{X\cdots N}$) has a more linear than monotonic correlation with the other properties (Figures 2 and S1, 4th row and 5th column in the right panel). The exceptions to this are the X$\cdots$N dipole moment ($\mu_{X\cdots N}$) and C–X dipole moment in the XB donor (μ^{donor}_{C-X}), which are slightly more monotonic than linear. This can be seen from the pair plot data in Figure S6 (6th and 8th rows in the 5th column) that is more exponential than linear. In general, Figure S6 shows the density distributions (5th column) associated with $R_{X\cdots N}$ for each halogen atom are very broad and overlapping in the center of the graph. This evidence supports the fact, introduced by Kraka et al.,[70] that although knowing the bond length can be helpful in prediction, the bond length is not necessarily indicative of bond strength. The change

in the C–X bond length upon complexation (ΔR_{C-X}), however, has a slightly more monotonic and linear relationship with all variables (5th row and 6th column in the right panel of Figures 2 and S1) when compared to $R_{X\cdots N}$ (4th row and 5th column in the right panel of Figures 2 and S1). The values of ΔR_{C-X} are found to be positive, and while not absolute, this typically suggests that the bond strength becomes weaker upon complexation. While this logical assertion is not supported by high correlations ($|rs| \leq 0.78$, $|r| \leq 0.80$), ΔR_{C-X} is negatively correlated to Δk^a_{C-X} (5th row of 4th column in right panel of Figures 2 and S1). This demonstrates that as the C–X bond becomes longer upon complexation, the C–X bond does, in fact, get weaker. Upon complexation, a charge transfer occurs from the lone pair of the nitrogen atom in ammonia to the σ^* orbital of the C–X bond in XB donor. This charge transfer increases the electron density in the C–X bond, causing the repulsive forces between electrons to increase, resulting in the C–X elongating and becoming weaker. Along with these observations, there is a clear linear and monotonically negative trend between ΔR_{C-X} and E_{bind} ($r = -0.97$, $rs = -0.94$). As E_{bind} becomes increasingly more negative, the C–X bond length elongates causing the change in C–X bond length to be increasingly more positive. One way to think about this occurrence is that when the orbitals containing the lone pair electrons of the Lewis base overlaps with the σ^* orbital of the C–X bond in the XB donor, an initial charge transfer from the lone pair to the C–X σ^* orbital occurs. This charge transfer, in conjunction with a back donation of electrons from the covalently bonded R group, is redistributed into the molecular orbitals that make up the C–X bond, increasing the repulsive forces between the electrons and elongating the bond. Like E_{bind}, $V_{S,max}$ also has a very linear, monotonic correlation with ΔR_{C-X} ($r = 0.98$, $rs = 0.98$). The positive correlations for these two properties found in Figures 2 and S1 show that the change in the C–X bond length increases as $V_{S,max}$ increases. More attractive (positive) σ-holes will induce a larger effect on the C–X bond due to a stronger "pull" on the lone pair electrons from the Lewis base.

The C–X dipole moments (μ_{C-X}) do not have very strong correlations to the other

properties recorded. However, there are some interesting trends to be pointed out for the X$\cdots$N dipole moment ($\mu_{X\cdots N}$) against the other recorded properties. The most correlated property to $\mu_{X\cdots N}$ is E_{bind}. Figure 2 and Figure S1 show that the $\mu_{X\cdots N}$ vs. E_{bind} are monotonically increasing ($rs = 0.96$) and are mostly linear ($r = 0.88$). Meaning that as the X$\cdots$N dipole moment becomes increasingly more negative, the binding energy also becomes more negative. Dipole moments are known to arise between differences in electronegativity; the larger the difference in electronegativity, the larger the dipole. Therefore, the X$\cdots$N dipole becoming more negative implies that the attraction between the halogen and the N in ammonia increases. This increase in the attractive interactions means that the XB donor is holding onto the acceptor's electrons more strongly, thus allowing for a larger binding energy. Following this explanation, the trends between $\mu_{X\cdots N}$ and $V_{S,max}$ as well as $k^a_{X\cdots N}$ are somewhat easy to understand by chemical intuition.

Halo-alkyne Systems

The archetype systems presented above provide a general understanding regarding the behavior of XB donors that contain electron donating substituents. However, "real" systems tend to possess other molecular characteristics that can affect halogen bonding. Halo-alkynes are the logical next step in studying realistic XB systems because they are larger than the archetype XB donors and introduce π-bonds as well as unhybridized p-orbitals that interact with the halogen atom.

The distance of the σ-hole shows a higher degree of correlation to the other properties in the halo-alkyne systems than that of the archetype systems. While $V_{max}(r)$ may be correlated with the other properties based on Spearman (Fig. 3, left panel, 2nd column) and Pearson (Fig. S2, left panel, 2nd column) correlation, this is because it is highly dependent on the bonding environment and polarization of the halogen atom, which affect the other properties as well, especially the $V_{S,max}$. Additionally, larger halogen atoms utilize pseudopotentials, which can obscure the precise location of the halogen atom's geometric center

causing some inherent error when calculating $V_{max}(r)$.

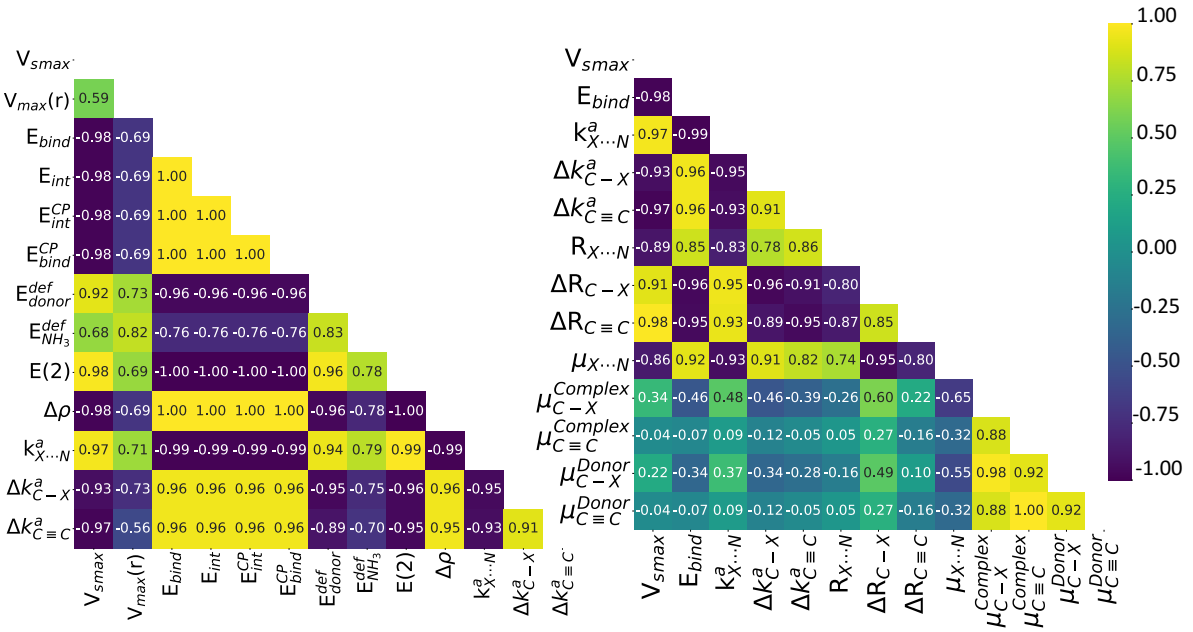

Figure 3: Spearman correlation heat map of the electronic and spectroscopic properties (left) and structural and spectroscopic properties (right) for the 20 halo-alkyne XB donors and corresponding complexes.

As expected, Figure 3 shows almost all Spearman correlations increase when moving from the archetypes to the halo-alkyne XB donors. Part of the reason for the increase in correlations is due to the increased polarization that occurs on the halogen atom, which is the result of the unhybridized p-orbitals from the alkyne carbon atom interacting with the p-orbitals of the halogen. $V_{S,max}$ benefits greatly from the increased polarization, as the electrons have more room for redistribution, causing the magnitude of the σ-hole to become more positive. The more positive σ-hole magnitude yields an increased attraction between the XB donor and the lone pair electrons of ammonia acceptor. The interaction induces a charge redistribution by pulling electron density from the nitrogen into the C–X bond of the XB donor. The stronger the attraction on those electrons, the more charge transfer that occurs. This in turn requires energy to extract electron density from the N atom and causes the C–X and C≡C bonds to weaken due to the increased repulsion forces that accompany

the addition of the electrons. The charge transfer into the XB donor modifies its electronic structure, producing higher deformation energies. These trends are supported by the high Spearman correlations presented in Figure 3 between $V_{S,max}$ (both panels, 1st column) and the binding/interaction energies, X$\cdots$N local force constant and bond length, magnitude of charge transfer, second order NBO perturbation energy for the donation of N lone pair electrons to the σ^* orbital of the C–X bond, change in the C–X and C$\equiv$C local force constants and bond lengths upon complexation, and XB donor deformation energy, respectively. This description also helps explain the total spread of the data in the density plots in Figure S7. Note, the distributions for $V_{S,max}$ representing each halogen atom (Figure S7, left column) are of moderate width with some overlapping regions; however, the distributions for the binding and interaction energies (colunns 3-6) are narrower with minimal overlap. The $V_{S,max}$ density curves for each halogen atom being moderately broad shows that the XB donors span a wide array of values. The overlapping regions indicate that for a specific range of $V_{S,max}$ values, there is a choice of halogen atom and backbone structures that fall within that range. The energetic distributions being relatively narrow with minimal overlap limits the range of binding/interaction of complexes formed with a specific halogen atom and what XB donors can be used for a certain halogen bond strength. The density plots for the XB donor deformation energy, second order NBO perturbation energy for the donation of N lone pair electrons to the σ^* orbital of the C–X bond, magnitude of charge transfer from the XB acceptor to the XB donor, and the X$\cdots$N local force constant show similarly narrow distributions with minimal overlap (Fig. S7, columns 7, 9-11). This illustrates that although the degree of attraction ($V_{S,max}$) can be manipulated through a wide array of XB donors, the electronic structure and characteristics of each donor are very important when considering the target properties and strength of the interactions of a XB complex for supramolecular aggregation, crystal engineering, and catalysis.

Focusing more on the structural aspects of the XB donors and complexes, the distributions for the X$\cdots$N bond length are fairly broad and overlap quite a bit with each other (Fig.

S8, 6th column). Chlorine XB donors form the longest X···N bonds, while astatine forms the smallest. This is more clearly displayed in Table 2, where the X···N bond lengths range from 2.87−2.90 Å for astatine donors and 2.98−3.02 Å for chlorine donors. The values for the X···N bond length in Table 2 and the density plots showing a good amount of overlap in Figure S8 again hint that the strongest bond is not always the shortest. This is further illustrated by the relative ordering of distributions in $R_{X\cdots N}$ versus E_{bind} and $k^a_{X\cdots N}$ (Fig. S8, columns 6, 2, and 3, respectively). There is a clear distinction where bromine-containing XB donors sometimes form shorter bonds than iodine-containing donors; however, the iodine donors have more negative binding energies and more positive X···N local force constants (Table 2). This shows the iodine-containing donors form the stronger bonds between bromine and iodine, but not always the shortest bonds. Polarization of the halogen atom plays a large role here. The polarization of iodine, which is already much greater than that of bromine, is enhanced due to the interaction of the unhybridized *p*-orbitals from the *sp*-hybridized carbon atoms bound to the halogen atom. So while all of the bromine-containing XB donors in Table 2 have shorter bonds than the analogous iodine-containing XB donors, none of bromine XB donors have more positive $V_{S,max}$ values. Iodine donors are typically able to have a more significant orbital overlap with XB acceptors than the bromine counterparts, which is a main governing factor in how strongly the molecules interact. This results in more negative binding energies and more positive X···N local force constants in the iodine-containing XB donors when compared to bromine-containing donors, despite having longer bonds. Another descriptor that may be used to help determine the strength of the halogen bonding interaction is the difference of the $R_{X\cdots N}$ bond length and the sum of the halogen and nitrogen atoms' van der Waals radii ($R - \Sigma r_{vdW}$). This descriptor essentially gives the amount of overlap that occurs between the halogen and nitrogen atoms when the noncovalent interaction is formed. The chlorine is seen to have the smallest amount of overlap, while the astatine atom has the largest amount of overlap. The amount of X···N overlap between iodine and bromine can be more easily seen through this value as well. The $R - \Sigma r_{vdW}$ value

shows that the iodine has more orbital overlap compared to the bromine atom, leading to more negative binding energies and stronger complexes.

Table 2: Magnitude of σ-hole ($V_{S,max}$; kcal mol^{-1}), X$\cdots$N bond length ($R_{X\cdots N}$; Å), change in the C–X bond length upon complexation (ΔR_{C-X}; Å), change in the C≡C bond length upon complexation ($\Delta R_{C\equiv C}$; Å), X$\cdots$N bond local force constant ($k^a_{X\cdots N}$; mDyn/Å), binding energy (E_{bind}; kcal mol^{-1}), charge transfer ($\Delta\rho$; me$^-$), and the difference between the halogen bond interaction length and the sum of the van der Waals radii ($R-\Sigma r_{vdW}$; Å) for the halo-alkyne systems.

XB Donor	$V_{S,max}$	$R_{X\cdots N}$	ΔR_{C-X}	$\Delta R_{C\equiv C}$	$k^a_{X\cdots N}$	E_{bind}	$\Delta\rho$	$R-\Sigma r_{vdW}$
				chlorine				
ClCCH	20.9	2.99	0.004	0.001	0.116	−3.09	−0.010	−0.86
ClCCOH	16.4	3.01	0.004	0.001	0.106	−2.55	−0.009	−0.84
$ClCCNH_2$	13.9	3.02	0.004	0.001	0.098	−2.29	−0.008	−0.83
$ClCCBH_2$	24.3	2.98	0.003	0.001	0.123	−3.48	−0.010	−0.87
$ClCCCH_3$	16.0	3.02	0.003	0.001	0.112	−2.51	−0.008	−0.83
				bromine				
BrCCH	29.1	2.93	0.012	0.001	0.169	−5.22	−0.023	−1.05
BrCCOH	25.0	2.94	0.012	0.001	0.166	−4.72	−0.022	−1.04
$BrCCNH_2$	22.2	2.96	0.011	0.001	0.162	−4.37	−0.020	−1.02
$BrCCBH_2$	32.5	2.92	0.011	0.002	0.172	−5.62	−0.024	−1.06
$BrCCCH_3$	24.2	2.96	0.007	0.001	0.161	−4.56	−0.020	−1.02
				iodine				
ICCH	35.7	2.96	0.022	0.002	0.185	−7.37	−0.039	−1.21
ICCOH	31.8	2.96	0.022	0.002	0.180	−6.87	−0.037	−1.21
$ICCNH_2$	28.9	2.99	0.021	0.001	0.176	−6.41	−0.034	−1.18
$ICCBH_2$	38.7	2.95	0.022	0.002	0.190	−7.76	−0.040	−1.22
$ICCCH_3$	30.8	2.98	0.021	0.002	0.196	−6.63	−0.035	−1.19
				astatine				
AtCCH	48.3	2.88	0.036	0.002	0.289	−10.30	−0.054	−1.38
AtCCOH	44.8	2.89	0.035	0.002	0.285	−9.81	−0.053	−1.37
$AtCCNH_2$	41.5	2.90	0.033	0.002	0.272	−9.25	−0.050	−1.36
$AtCCBH_2$	51.2	2.87	0.037	0.003	0.292	−10.75	−0.056	−1.39
$AtCCCH_3$	43.2	2.90	0.033	0.002	0.257	−9.46	−0.050	−1.36

The density distributions for the change in the C≡C bond length upon complexation overlap a great deal (Figure S8, 8th column). This agrees with the data for $\Delta R_{C\equiv C}$ provided in Table 2, which shows very small, comparable changes in the C≡C bond length that get slightly more positive as the size and polarization of the halogen atom increases. The elongation of the C≡C bond that occurs upon complexation results from the transfer of

electron density from the C–X π bonding orbitals and halogen lone pair electrons into C≡C σ^* and π^* antibonding orbitals. The right panel of Figure 4 shows that there is a trend ($rs = -0.95$) of increasing charge transfer from the ammonia nitrogen atom to the XB donor as the C≡C bond elongates. The additional electron density being introduced repels the halogen lone pairs, pushing them more towards the *sp*-hybridized carbon bonded to the halogen atom. This allows for more efficient redistribution of the electron density into the anti-bonding orbitals of the C≡C bond, increasing the repulsion of the electrons in the bonding region and elongating the bond. Note, however, the R group (R = H, OH, NH_2, BH_2, CH_3) is also contributing electron density to the C≡C bond. For example, the XB donors with the BH_2 group have the largest $\Delta R_{C\equiv C}$ due to the electron density being directed toward the C≡C bond (Table 2). The OH and NH_2 substituents, on the other hand, have dipole moments that orient away from the C≡C group. Thus, the amount of electron density transferred from these groups to the C≡C bond is limited.

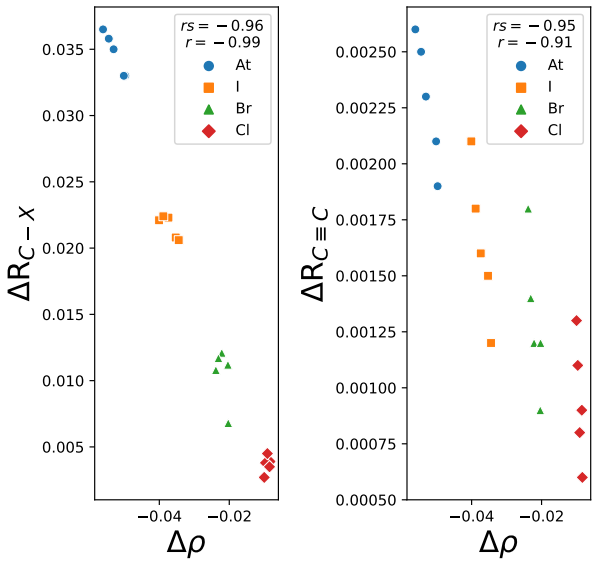

Figure 4: Change in C–X bond length upon complexation (ΔR_{C-X}; Å) and change in the C≡C bond length upon complexation ($\Delta R_{C\equiv C}$; Å) against the magnitude and direction of the charge transfer ($\Delta\rho$; me^-) for the halo-alkyne systems.

The C–X bond, however, is much more reliant on the electron transfer from the ammonia acceptor, and it differs greatly based on the identity of the halogen atom. Table 2 shows

that the change in the C–X bond length upon complexation becomes more positive as the size and polarizability of the halogen increases. This trend is also reflected by the negative correlation ($rs = -0.96$) in left panel of Figure 4. The tight grouping of the XB donors by halogen atom indicates the identity of the R group opposite the C≡C bond does not contribute as significantly to ΔR_{C-X} as the identity of the halogen atom. This is because the electron density from the R group would have to migrate a substantial distance across multiple atomic sites to move into the bonding region of the the C–X bond. Whereas, the electron density from the halogen atom, as well as the electron density transferred into the halogen atom upon complexation, does not have to travel far to influence the C–X bond. Larger halogen atoms are able to redistribute more electron density into the C–X bond than smaller halogens, resulting in notable bond elongation. This is due to the increase in polarization of the halogen atom as the size of the atom increases. The transfer of electron density from the ammonia acceptor to the halogen atom is also facilitated by increased polarizability, leading to more electron density being transferred from the N lone pair to the σ^* orbital of the C–X bond. Hence, the identity of the halogen atom is the largest contributor to the elongation of the C–X bond in the XB donor upon complexation. This observation is also seen from the change in the C–X bond vibrational frequencies (Table S1) becoming more negative as the size of the halogen atom becomes larger.

Halo-benzene Systems and Halo-ethynyl Benzene Systems

While XB donors with an alkyne backbone elucidate how unhybridized p orbitals affect the polarization of the halogen atom and allow for the EDG to act as intended, resonance and induction effects are absent in these systems. Here we investigate halo-benzene and halo-ethynyl benzene systems (Figure 1c,d) to determine the effects of electron density delocalization in a ring system on the XB donor and the corresponding complexes.

Similar to the alkyne systems, the σ-hole distance (Figs. 5, S3, 6, and S4) was found to have a moderate correlation to all other properties recorded for the halo-benzene and

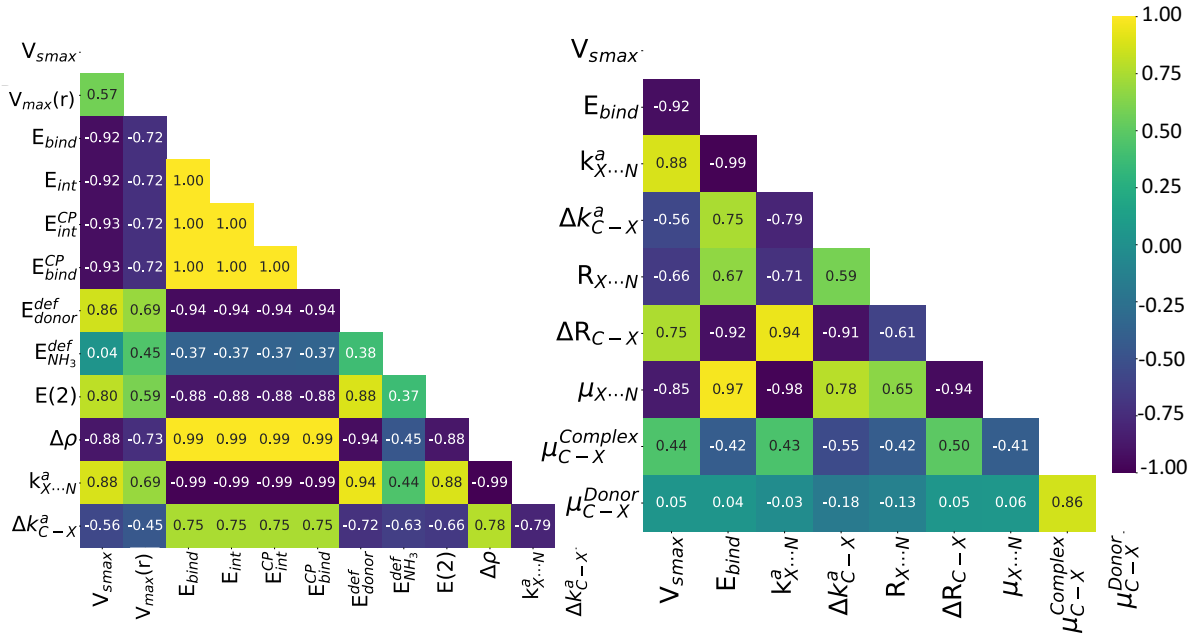

Figure 5: Spearman correlation heat map of the electronic and spectroscopic properties (left) and structural and spectroscopic properties (right) for the 200 halo-benzene XB donors and corresponding complexes.

halo-ethynyl benzene systems. However, as stated in previous sections, the size and the polarization of the halogen atom is the determining factor of the calculated σ-hole distance. $V_{S,max}$, however, is linearly and monotonically correlated to most of the other properties recorded through clear relationships. This assertion follows from explanations described in previous sections and is further supported by the distinct variations in properties as the value of $V_{S,max}$ is modulated. Table 3 shows a clear difference in the values of $V_{S,max}$ and E_{bind} for the halo-benzene systems compared to the alkyne systems (Table 2) and halo-ethynyl benzene systems (Table 4). The latter two system types have notably larger magnitudes. The discrepancies can be illustrated by focusing on the halo-benzene and halo-alkyne systems, where there is an increase of p-character in the hybridization of the carbon atom bonded to the halogen in the halo-benzene systems. The sp^2 hybridized carbon has one less unhybridized p orbital able to interact with the halogen atom, thus the polarization of the halogen atom in the halo-benzene systems is less than that of the halo-alkyne systems.

Table 3: Electron donating group (EDG), position of EDG on benzene ring, magnitude of σ-hole ($V_{S,max}$; kcal mol^{-1}), X$\cdots$N bond length ($R_{X\cdots N}$; Å), change in the C–X bond length upon complexation (ΔR_{C-X}; Å), change in the C–X frequency upon complexation ($\Delta\nu_{C-X}$; cm^{-1}), binding energy (E_{bind}; kcal mol^{-1}), charge transfer ($\Delta\rho$; me$^-$), and the difference between the halogen bond interaction length and the sum of the van der Waals radii ($R - \Sigma r_{vdW}$; Å) for the halo-benzene systems.

EDG	position[a]	$V_{S,max}$	$R_{X\cdots N}$	ΔR_{C-X}	$\Delta\nu_{C-X}$	E_{bind}	$\Delta\rho$	$R - \Sigma r_{vdW}$
				chlorine				
H		4.1	3.15	−0.001	1	−1.23	−0.002	−0.70
OH	*o*	16.6	3.10	−0.002	0	−2.26	−0.007	−0.75
	m	6.6	3.14	−0.003	0	−1.20	−0.006	−0.71
	p	3.3	3.15	−0.001	1	−1.23	−0.002	−0.70
NH_2	*o*	6.1	3.15	−0.002	1	−1.55	−0.002	−0.70
	m	0.3	3.22	−0.000	0	−1.23	−0.000	−0.63
	p	0.8	3.20	−0.000	1	−1.18	−0.001	−0.65
BH_2	*o*	4.2	3.13	−0.005	1	−1.20	−0.006	−0.72
	m	7.8	3.12	−0.003	0	−1.40	−0.007	−0.73
	p	8.0	3.12	−0.003	0	−1.39	−0.006	−0.73
				bromine				
H		10.9	3.08	0.000	−2	−2.49	−0.015	−0.90
OH	*o*	22.9	3.05	0.001	−1	−3.80	−0.017	−0.93
	m	13.4	3.07	0.000	−1	−2.72	−0.015	−0.91
	p	10.2	3.08	0.001	−2	−2.42	−0.014	−0.90
NH_2	*o*	12.2	3.10	0.000	2	−2.53	−0.013	−0.88
	m	7.0	3.10	−0.001	−1	−2.11	−0.013	−0.88
	p	7.5	3.10	0.000	−2	−2.16	−0.014	−0.88
BH_2	*o*	10.3	3.07	−0.002	−1	−2.59	−0.015	−0.91
	m	14.6	3.06	−0.003	−2	−2.95	−0.016	−0.92
	p	14.6	3.06	0.000	−2	−2.91	−0.016	−0.92
				iodine				
H		16.1	3.12	0.004	−4	−4.03	−0.025	−1.05
OH	*o*	27.5	3.09	0.005	−3	−5.33	−0.028	−1.08
	m	18.7	3.11	0.004	−2	−4.31	−0.026	−1.06
	p	15.6	3.12	0.004	−3	−3.98	−0.024	−1.05
NH_2	*o*	16.9	3.15	0.003	−1	−3.89	−0.022	−1.02
	m	12.3	3.14	0.003	−3	−3.58	−0.023	−1.03
	p	12.9	3.14	0.004	−3	−3.67	−0.023	−1.03
BH_2	*o*	15.0	3.11	0.003	−3	−4.04	−0.026	−1.06
	m	19.9	3.09	0.004	−2	−4.57	−0.027	−1.08
	p	19.7	3.10	0.004	−3	−4.49	−0.026	−1.07
				astatine				
H		24.0	3.06	0.009	−5	−5.79	−0.034	−1.20
OH	*o*	35.7	3.03	0.011	−5	−7.24	−0.038	−1.23
	m	26.7	3.04	0.010	−5	−6.13	−0.036	−1.22
	p	23.7	3.05	0.009	−5	−5.76	−0.034	−1.21
NH_2	*o*	24.6	3.08	0.008	−4	−5.64	−0.032	−1.18
	m	20.0	3.07	0.007	−4	−5.28	−0.032	−1.19
	p	20.9	3.07	0.008	−4	−5.40	−0.032	−1.19
BH_2	*o*	22.9	3.04	0.008	−4	−5.92	−0.036	−1.22
	m	28.0	3.03	0.010	−3	−6.43	−0.037	−1.23
	p	27.7	3.04	0.009	−5	−6.30	−0.036	−1.22

[a] *o* = ortho, *m* = meta, *p* = para

Another factor is the delocalization of electrons in the benzene ring, which allows for back-donation of electron density from the ring to the halogen atom. This back-donation of electron density increases the electron repulsion around the halogen atom thus decreasing its polarizability. Hence, a less positive $V_{S,max}$ forms on the cap of the C–X bond. The addition of EDGs bonded to the benzene ring increases the electron density in the ring even further. This allows for more electron density to be delocalized in the ring, more back-donation to the halogen atom, and thus the polarization of the halogen atom is further reduced. Hence, the additional electron density in the ring generally hinders formation of an intense σ-hole, as is supported by smaller $V_{S,max}$ values for the more donating substituents in Table 3. However, when EDGs are *ortho* to the halogen atom, intramolecular hydrogen bond interactions may also occur, depending upon the identity of the substituent and the orientation of its hydrogen atoms. These interactions promote further polarization of the halogen atom, generating a more positive $V_{S,max}$ and larger E_{bind} compared to EDGs in the *meta* or *para* positions. The side interactions, known as hydrogen bond enhanced halogen bonds (HBeXB), have been reported to improve the interaction strength and stability of XB complexes in the literature.[22–27,29,30,71] The BH_2 substituent is the exception to this trend. When at the *ortho* position, it yields the smallest $V_{S,max}$ and weakest E_{bind} compared to *meta* or *para* positions that are comparable. BH_2 has less polar bonds that are polarized the opposite direction compared to the other EDGs, which deters hydrogen bonding and makes the *ortho* site the least favorable.

Table 4 shows similar trends exist in the halo-ethynyl benzene systems. More polar EDGs in the *ortho* position generate the largest $V_{S,max}$ and most stable complexes. However, in these systems, the hydrogen atoms interact with the ethynyl (C≡C) group rather than the halogen atom directly. The *sp* hybridized carbon of the ethynyl linker enhances the polarization of the halogen atoms, as described in the previous section with the halo-alkyne systems, and the halogen atom is further polarized when additional interactions with the ethynyl linker are possible. This can be seen in Table 4 with increased $V_{S,max}$ and stability when the

more polar EDGs are *ortho* to the principle halogen atom and the larger magnitudes associated with the halo-ethynyl benzene donors compared to the halo-benzene donors (Table 3). Moreover, the introduction of the ethynyl linker generates a smaller spread of $V_{S,max}$ values for different halogens. This is reflected in tighter distributions with less overlap in the density plots for the halo-ethynyl benzene XB donors (Figures S11 and S12, left column) compared to the halo-benzene XB donors (Figures S9 and S10, left column). The spread in the data is not only influenced by the hydrogen bond-like interactions described above between the EDGs and the halogen atom or ethynyl linker, but also because of repulsive interactions between lone pair electrons in the EDG and the ethynyl linker or the electronegative belt that surrounds the halogen atom. The halo-benzene donors are affected much more by these repulsive interactions due to geometric constraints and the generally lower levels of halogen atom polarization present. For these reasons, the halo-ethynyl benzene XB systems have a much more monotonic and linear correlation between the $V_{S,max}$ and all other properties compared to the halo-benzene XB systems (Figures 5 and 6; Figures S3 and S4).

Table 4: Electron donating group (EDG), position of EDG on benzene ring, magnitude of σ-hole ($V_{S,max}$; kcal mol^{-1}), X$\cdots$N bond length ($R_{X\cdots N}$; Å), change in the C–X bond length upon complexation (ΔR_{C-X}; Å), change in the C–X frequency upon complexation ($\Delta\nu_{C-X}$; cm^{-1}), change in the C≡C bond length upon complexation ($\Delta R_{C\equiv C}$; Å), change in the C≡C frequency upon complexation ($\Delta\nu_{C\equiv C}$; cm^{-1}), binding energy (E_{bind}; kcal mol^{-1}), charge transfer ($\Delta\rho$; me$^-$), and the difference between the halogen bond interaction length and the sum of the van der Waals radii ($R-\Sigma r_{vdW}$; Å) for the halo-ethynyl benzene systems.

EDG	position[a]	$V_{S,max}$	$R_{X\cdots N}$	ΔR_{C-X}	$\Delta\nu_{C-X}$	$\Delta R_{C\equiv C}$	$\Delta\nu_{C\equiv C}$	E_{bind}	$\Delta\rho$	$R-\Sigma r_{vdW}$
					chlorine					
H		18.6	3.00	0.003	0	0.001	−8	−2.84	−0.009	−0.85
OH	*o*	26.1	2.97	0.004	−2	0.001	−8	−3.64	−0.011	−0.88
	m	20.4	3.00	0.003	1	0.001	−7	−2.97	−0.009	−0.85
	p	17.4	3.01	0.003	1	0.001	−7	−2.71	−0.009	−0.84
NH_2	*o*	19.4	3.00	0.003	−2	0.001	−5	−2.88	−0.009	−0.85
	m	16.4	3.01	0.003	0	0.001	−7	−2.63	−0.009	−0.84
	p	15.4	3.01	0.003	1	0.001	−6	−2.52	−0.009	−0.84
BH_2	*o*	19.4	2.99	0.003	0	0.001	−9	−3.00	−0.010	−0.86
	m	21.3	2.99	0.003	1	0.001	−8	−3.11	−0.010	−0.86
	p	21.6	2.99	0.003	2	0.001	−8	−3.15	−0.010	−0.86
					bromine					
H		26.7	2.94	0.01	−4	0.001	−9	−4.95	−0.022	−1.04
OH	*o*	34.1	2.90	0.013	−1	0.001	−9	−5.92	−0.026	−1.08
	m	28.4	2.93	0.011	−1	0.001	−10	−5.10	−0.023	−1.05
	p	25.5	2.94	0.011	−2	0.001	−8	−4.80	−0.022	−1.04
NH_2	*o*	27.3	2.93	0.011	−1	0.001	−8	−5.01	−0.023	−1.05
	m	24.3	2.95	0.011	−2	0.001	−9	−4.69	−0.21	−1.03
	p	23.4	2.95	0.011	−2	0.001	−8	−4.58	−0.021	−1..03
BH_2	*o*	27.5	2.93	0.011	−1	0.001	−11	−5.14	−0.023	−1.05
	m	29.3	2.93	0.011	−3	0.001	−10	−5.27	−0.023	−1.05
	p	29.7	2.92	0.011	−3	0.002	−11	−5.31	−0.023	−1.06
					iodine					
H		33.0	2.96	0.022	−8	0.002	−11	−7.05	−0.038	−1.21
OH	*o*	40.5	2.92	0.025	−6	0.002	−10	−8.19	−0.044	−1.25
	m	34.7	2.96	0.022	−6	0.002	−11	−7.23	−0.038	−1.21
	p	31.8	2.97	0.021	−6	0.001	−11	−6.88	−0.037	−1.20
NH_2	*o*	33.7	2.96	0.022	−5	0.001	−9	−7.12	−0.038	−1.21
	m	30.6	2.97	0.021	−5	0.002	−10	−6.76	−0.036	−1.20
	p	29.7	2.98	0.020	−6	0.001	−9	−6.62	−0.035	−1.19
BH_2	*o*	33.8	2.96	0.022	−5	0.002	−13	−7.26	−0.039	−1.21
	m	35.6	2.95	0.022	−4	0.002	−11	−7.43	−0.040	−1.22
	p	36.0	2.95	0.022	−7	0.002	−12	−7.47	−0.040	−1.22
					astatine					
H		45.7	2.89	0.035	−10	0.002	−14	−9.99	−0.053	−1.37
OH	*o*	53.6	2.85	0.040	−9	0.002	−13	−11.36	−0.061	−1.41
	m	47.4	2.88	0.036	−8	0.002	−14	−10.20	−0.054	−1.38
	p	44.4	2.89	0.034	−8	0.002	−13	−9.79	−0.052	−1.37
NH_2	*o*	46.5	2.88	0.036	−7	0.002	−12	−10.09	−0.054	−1.38
	m	43.2	2.89	0.034	−8	0.002	−13	−9.65	−0.052	−1.37
	p	42.3	2.90	0.033	−8	0.002	−12	−9.49	−0.051	−1.36
BH_2	*o*	46.5	2.88	0.036	−7	0.002	−15	−10.23	−0.054	−1.38
	m	48.2	2.88	0.036	−7	0.002	−14	−10.43	−0.056	−1.38
	p	48.6	2.87	0.037	−8	0.003	−15	−10.49	−0.056	−1.39

[a] *o* = ortho, *m* = meta, *p* = para

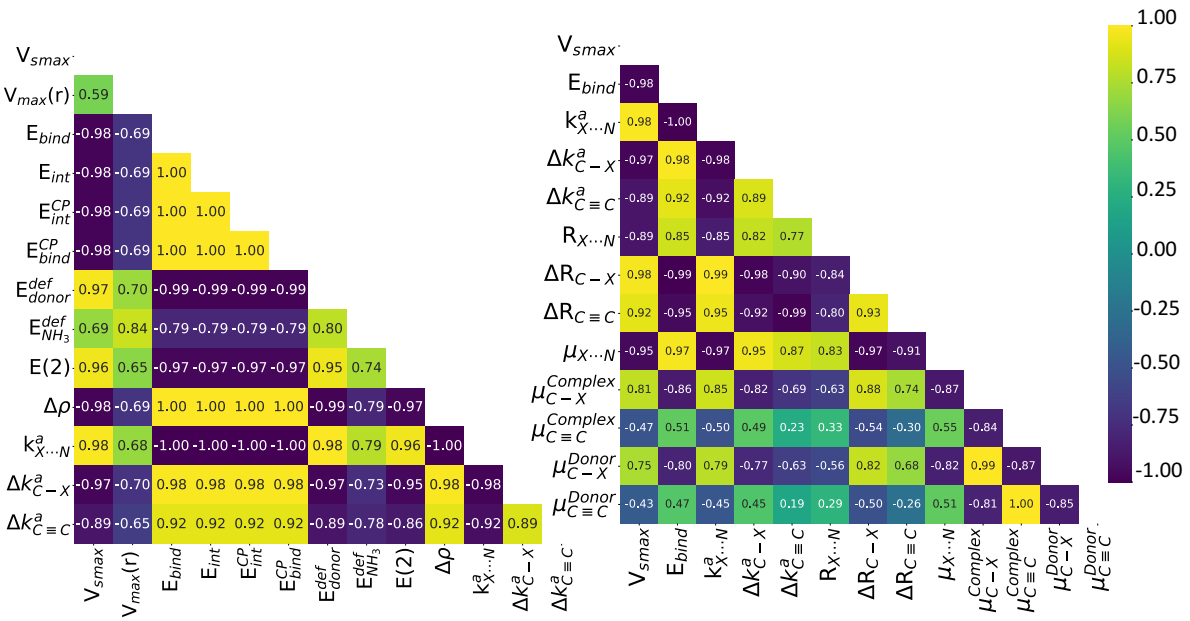

Figure 6: Spearman correlation heat map of the electronic and spectroscopic properties (left) and structural and spectroscopic properties (right) for the 204 halo-ethynyl benzene XB donors and corresponding complexes.

Falling in line with $V_{S,max}$, the interaction and binding energies, and the charge transfer also have much more monotonic (Figure 6) and linear (Figure S4) correlations against all properties recorded in the halo-ethynyl benzene systems compared to the halo-benzene systems (Figures 5 and S3). And tighter distributions with less overlap are found for these properties upon introducing an ethynyl linker (Figures S11 and S12 versus Figures S9 and S10). These observations can simply be explained through the degree of correlation and spread of $V_{S,max}$ values for the ring systems. Since there is a larger spread of $V_{S,max}$ values in the halo-benzene systems, there will be more variations in the extent of attraction between the Lewis base (ammonia) and these XB donors, which mutes/spreads the energetics and charge transfer upon complexation. Therefore, the halo-ethynyl benzene systems, which have a smaller spread and larger $V_{S,max}$ values, will also generate analogous results in highly correlated properties upon XB complex formation, such as E_{bind} and $\Delta\rho$.

Returning briefly to the positional dependence of the electron donating substituents,

Tables 3 and 4 both show that hydroxyl and amine EDGs in the *ortho* position yield a much more positive $V_{S,max}$ when compared to other sites, and E_{bind} is more negative as well. These configurations form stronger complexes for both the halo-benzene and halo-ethynyl benzene donors and highlight the utility of supplementary forces when considering molecular design of XB interactions. However, the trends are not absolute for these donors when considering EDGs at other locations. The halo-ethynyl benzene donors show uniform agreement that these EDGs in the *ortho* position are best in terms of $V_{S,max}$ and E_{bind}, followed by the *meta* position, and then *para* (i.e., $o > m > p$). As discussed above, additional hydrogen bonding interactions are possible from the *ortho* site that effectively increase the polarization of the halogen atom leading to enhanced binding. EDGs *meta* to the principle halogen atom form a dipole moment pointing away from the benzene ring, and while they supplement electron density into the ring, the two substituents also pull more electron density away from the halogen atom, decreasing the magnitudes of $V_{S,max}$ and E_{bind}. A similar effect occurs with EDGs in the *para* position, but to a lesser extent due to there only being a single substituent. Another point to be made is the ethynyl linker in the halo-ethynyl benzene donors serves as a sort of barrier, or steric factor, protecting the halogen atom against distortions in electron density from the benzene ring. The halo-benzene donors, on the other hand, are in disagreement on the relative ordering beyond the *ortho* position. Halo-benzene donors with hydroxyl EDGs follow the trends noted above (i.e., $o > m > p$), whereas Table 3 shows different behavior when the EDG is an amine; the magnitudes of $V_{S,max}$ and E_{bind} are greater for *para* than *meta* (i.e., $o > p > m$). A reason for the different behavior could be due to the weaker dipoles of the amine groups coupled with induction and resonance. More electron density is being donated back into the benzene from the two amine groups in the *meta* position rather than the single amine in the *para* position. The increase in electron density then repels the electronegative belt around the halogen atom, preventing a large σ-hole and a strong interaction with an XB acceptor from forming. While the data in Table 3 supports this ranking, it is worth noting that for each halogen, $V_{S,max}$ and E_{bind} are farily comparable

with amines at the *para* or *meta* positions.

As described above, the largest effects are found when hydroxyl and amine EDGs are located at the *ortho* position for both the halo-benzene and halo-ethynyl benzene donors. The inverted bond polarity of the BH_2 substituent generates entirely different behavior, where the *ortho* position is the least desireable in all cases due to unfavorable interactions with the halogen belt or ethynyl linker. Table 3 largely shows that for halo-benzene donors, the *meta* position forms the most positive σ-hole and largest E_{bind}, followed by the *para* position and then *ortho*. Table 4 shows that for halo-ethynyl benzene donors, the ordering for the BH_2 group is the *para* position followed by *meta* and then *ortho*. For both types of systems and all halogens, the results upon adding BH_2 groups to the *para* or *meta* positions are very comparable. The dissimilar behavior of BH_2, compared to the other EDGs under study, may result from the substituent effectively having more electron withdrawing characteristics. This is due to the hydrogen atoms being slightly more electronegative than boron, which causes some bond polarization toward the hydrogens. Therefore, the BH_2 substituents in the *meta* and *para* positions form dipole moments away from the halogen atom. The formation of bond dipoles pointing toward the hydrogen atoms in the BH_2 groups can also account for the muted hydrogen bonding with the halogen atom when placed in the *ortho* position.

Conclusions

A total of 448 halogen bond donors with varied electron donating substituents were examined systematically for their electronic and spectroscopic properties in monomeric form and upon complexation with ammonia. Statistical analyses were conducted upon each property to find monotonic and linear trends in the data, through a comparison of halogen atom identity (i.e., Cl, Br, I, At) and backbone of the R group (i.e., –H, –OH, $–NH_2$, $–BH_2$, $–CH_3$, –C≡CR, benzene, or ethynyl benzene) covalently bonded to the halogen atom in question.

Among all the XB donors studied, the halo-alkynes and halo-ethynyl benzene systems

were found to have the most positive $V_{S,max}$, allowing for stronger halogen bonds to form and more stable complexes. While the halo-benzene derivatives generally had less positive $V_{S,max}$ and formed weaker halogen bonds, donors with a more polar electron donating group in the *ortho* position produced intramolecular interactions between the halogen atom and the EDG. This allowed for a much more positive $V_{S,max}$ to form, therefore generating stronger interactions between the XB donor and ammonia acceptor. The additional interactions between the halogen atom and the EDGs *ortho* to the halogen caused a wide breadth of $V_{S,max}$ values, and consequently, interaction and binding energies in the halo-benzene systems. This occurrence was somewhat remedied through the addition of an ethynyl linker, causing the EDGs to interact with the ethynyl linker rather than directly with the halogen atom. Halo-ethynyl benzene donors with hydrogen bonding between the ethynyl linker and hydrogen atoms from EDGs in the *ortho* position formed the most positive σ-holes for the hydroxyl and amine substituents. The BH_2 substituent yielded the most positive $V_{S,max}$ and most negative E_{bind} when in the *para* position for the halo-ethynyl benzene donors and in the *meta* position for the halo-benzene donors.

Throughout the study, $V_{S,max}$ was found to correlate very well monotonically and linearly with the other electronic and spectroscopic properties recorded. The same is true for the interaction and binding energies, magnitude of charge transferred upon complexation, and the X$\cdots$N bond local force constant. This demonstrates that electrostatic and electronic properties of the XB donors are particularly important when considering molecular and material design. Supported with the knowledge and insight gained throughout this work we aim to extend these investigations to include XB systems with cooperative electron withdrawing and electron donating group effects.

Acknowledgement

The authors were supported by the National Science Foundation (NSF) under award num-

ber 2147956. The authors thank Baylor University High Performance Research Computing services for their generous allocation of computational resources on the Kodiak HPC cluster and the CATCO Research group for the use of the Local Mode Analysis code.

Supporting Information Available

The Supporting Information is available free of charge at https://xxxxx/yyy/zzz.

Computational details for select XB donors and complexes; Pearson correlation heat maps; Pair plots and density distributions.

Due to size constraints, raw data used for the statistical analyses as well as molecular coordinates and/or Gaussian checkpoint files can be provided upon request.

References

(1) Colin, M. Note sur quelques combinaisons de l'iode. *Ann. Chim* **1814**, *91*, 252–272.

(2) Colin, J. J.; Gaultier de Claubry, H. Sur le combinaisons de l'iode avec les substances végétales et animales. *Ann. Chim* **1814**, *90*, 87–100.

(3) Guthrie, F. XXVIII.—On the iodide of iodammonium. *Journal of the Chemical Society* **1863**, *16*, 239–244.

(4) Remsen, I.; Norris, J. Action of the halogens on the methylamines. *Am Chem J* **1896**, *18*, 90–95.

(5) Parisini, E.; Metrangolo, P.; Pilati, T.; Resnati, G.; Terraneo, G. Halogen bonding in halocarbon–protein complexes: a structural survey. *Chemical Society Reviews* **2011**, *40*, 2267–2278.

(6) Metrangolo, P.; Meyer, F.; Pilati, T.; Resnati, G.; Terraneo, G. Halogen Bonding in

Supramolecular Chemistry. *Angewandte Chemie International Edition* **2008**, *47*, 6114–6127.

(7) Politzer, P.; Murray, J. S.; Clark, T. Halogen bonding: an electrostatically-driven highly directional noncovalent interaction. *Physical Chemistry Chemical Physics* **2010**, *12*, 7748–7757.

(8) Bent, H. A. An Appraisal of Valence-bond Structures and Hybridization in Compounds of the First-row elements. *Chemical Reviews* **1961**, *61*, 275–311.

(9) Szczęśniak, M. M.; Chałasinski, G. Reassessing the Role of σ Holes in Noncovalent Interactions: It is Pauli Repulsion that Counts. *Frontiers in Chemistry* **2022**, *10*, 858946.

(10) Sakai, T.; Torii, H. Substituent Effect and Its Halogen-Atom Dependence of Halogen Bonding Viewed through Electron Density Changes. *Chemistry – An Asian Journal* **2023**, *18*, e202201196.

(11) Xu, Y.; Hao, A.; Xing, P. X$\cdots$X Halogen Bond-Induced Supramolecular Helices. *Angewandte Chemie International Edition* **2022**, *61*, e202113786.

(12) Cunha, A. V.; Havenith, R. W. A.; van Gog, J.; De Vleeschouwer, F.; De Proft, F.; Herrebout, W. The Halogen Bond in Weakly Bonded Complexes and the Consequences for Aromaticity and Spin-Orbit Coupling. *Molecules* **2023**, *28*, 772.

(13) Nziko, V. d. P. N.; Scheiner, S. Comparison of π-hole tetrel bonding with σ-hole halogen bonds in complexes of XCN (X = F, Cl, Br, I) and NH3. *Physical Chemistry Chemical Physics* **2016**, *18*, 3581–3590.

(14) Clark, T.; Hennemann, M.; Murray, J. S.; Politzer, P. Halogen bonding: the σ-hole. *Journal of Molecular Modeling* **2007**, *13*, 291–296.

(15) Politzer, P.; Murray, J. S.; Clark, T.; Resnati, G. The σ-hole revisited. *Physical Chemistry Chemical Physics* **2017**, *19*, 32166–32178.

(16) Desiraju, G. R.; Ho, P. S.; Kloo, L.; Legon, A. C.; Marquardt, R.; Metrangolo, P.; Politzer, P.; Resnati, G.; Rissanen, K. Definition of the halogen bond (IUPAC Recommendations 2013). *Pure and Applied Chemistry* **2013**, *85*, 1711–1713.

(17) Lapp, J.; Scheiner, S. Proximity Effects of Substituents on Halogen Bond Strength. *The Journal of Physical Chemistry A* **2021**, *125*, 5069–5077.

(18) Naghani, F. F.; Emamian, S.; Zare, K. Exploring influence of fluorine substitution on the strength and nature of halogen bond between iodobenzene and hydrogen cyanide. *Journal of Physical Organic Chemistry* **2021**, *34*, e4213.

(19) Tang, Q.; Li, Q. Non-additivity of F substituent in enhancing the halogen bond in C6H5I$\cdots$NCH. *Computational and Theoretical Chemistry* **2015**, *1070*, 21–26.

(20) Michalczyk, M.; Kizior, B.; Zierkiewicz, W.; Scheiner, S. Factors contributing to halogen bond strength and stretch or contraction of internal covalent bond. *Physical Chemistry Chemical Physics* **2023**, *25*, 2907–2915.

(21) Priimagi, A.; Cavallo, G.; Metrangolo, P.; Resnati, G. The Halogen Bond in the Design of Functional Supramolecular Materials: Recent Advances. *Accounts of Chemical Research* **2013**, *46*, 2686–2695.

(22) Riel, A. M. S.; Rowe, R. K.; Ho, E. N.; Carlsson, A.-C. C.; Rappé, A. K.; Berryman, O. B.; Ho, P. S. Hydrogen Bond Enhanced Halogen Bonds: A Synergistic Interaction in Chemistry and Biochemistry. *Accounts of Chemical Research* **2019**, *52*, 2870–2880.

(23) Sun, J.; Riel, A. M. S.; Berryman, O. B. Solvatochromism and fluorescence response of a halogen bonding anion receptor. *New Journal of Chemistry* **2018**, *42*, 10489–10492.

(24) Riel, A. M. S.; Decato, D. A.; Sun, J.; Massena, C. J.; Jessop, M. J.; Berryman, O. B. The intramolecular hydrogen bonded–halogen bond: a new strategy for preorganization and enhanced binding. *Chemical Science* **2018**, *9*, 5828–5836.

(25) Riel, A. M. S.; Decato, D. A.; Sun, J.; Berryman, O. B. Halogen bonding organocatalysis enhanced through intramolecular hydrogen bonds. *Chemical Communications* **2022**, *58*, 1378–1381.

(26) Decato, D. A.; Riel, A. M. S.; May, J. H.; Bryantsev, V. S.; Berryman, O. B. Theoretical, Solid-State, and Solution Quantification of the Hydrogen Bond-Enhanced Halogen Bond. *Angewandte Chemie International Edition* **2021**, *60*, 3685–3692.

(27) Scheiner, S. Enhancement of Halogen Bond Strength by Intramolecular H-Bonds. *The Journal of Physical Chemistry A* **2023**, *127*, 4695–4703.

(28) Scheiner, S. Ability of Peripheral H Bonds to Strengthen a Halogen Bond. *The Journal of Physical Chemistry A* **2022**, *126*, 9691–9698.

(29) Devore, D. P.; Ellington, T. L.; Shuford, K. L. Interrogating the Interplay between Hydrogen and Halogen Bonding in Graphitic Carbon Nitride Building Blocks. *The Journal of Physical Chemistry A* **2020**, *124*, 10817–10825.

(30) Ellington, T. L.; Devore, D. P.; Uvin G. De Alwis, W. M.; French, K. A.; Shuford, K. L. Shedding Light on the Vibrational Signatures in Halogen-Bonded Graphitic Carbon Nitride Building Blocks. *ChemPhysChem* **2023**, *24*, e202200812.

(31) Grabowski, S. J. Cooperativity of hydrogen and halogen bond interactions. 8th Congress on Electronic Structure: Principles and Applications (ESPA 2012) A Conference Selection from Theoretical Chemistry Accounts. 2014; pp 59–68.

(32) Esrafili, M. D.; Mohammadian-Sabet, F. Halogen-Bond Interactions Enhanced by

Charge-Assisted Hydrogen Bonds: An Ab Initio Study. *Bulletin of the Chemical Society of Japan* **2014**, *87*, 882–889.

(33) Esrafili, M. D.; Vakili, M. Strengthening halogen···halogen interactions by hydrogen and lithium bonds in NCM··· NCX··· YCH3 and CNM··· CNX··· YCH3 (M= H, Li and X, Y= Cl, Br) complexes: a comparative study. *Molecular Physics* **2016**, *114*, 325–332.

(34) An, X.; Yang, X.; Xiao, B.; Cheng, J.; Li, Q. Comparison of hydrogen and halogen bonds between dimethyl sulfoxide and hypohalous acid: Competition and cooperativity. *Molecular Physics* **2017**, *115*, 1614–1623.

(35) Del Bene, J. E.; Alkorta, I.; Elguero, J. Hydrogen and Halogen Bonding in Cyclic FH (4-n): FCl n Complexes, for n= 0–4. *The Journal of Physical Chemistry A* **2018**, *122*, 2587–2597.

(36) Ciancaleoni, G. Cooperativity between hydrogen-and halogen bonds: The case of selenourea. *Physical Chemistry Chemical Physics* **2018**, *20*, 8506–8514.

(37) Yao, F.; Gong, N.; Fang, W.; Men, Z. Spectroscopic evidence of a particular intermolecular interaction in iodomethane–ethanol mixtures: the cooperative effect of halogen bonding, hydrogen bonding, and the solvent effect. *Physical Chemistry Chemical Physics* **2020**, *22*, 5702–5710.

(38) Foster, J. P.; Weinhold, F. Natural hybrid orbitals. *Journal of the American Chemical Society* **1980**, *102*, 7211–7218.

(39) Reed, A. E.; Weinhold, F. Natural bond orbital analysis of near-Hartree–Fock water dimer. *The Journal of Chemical Physics* **1983**, *78*, 4066–4073.

(40) Reed, A. E.; Weinhold, F. Natural localized molecular orbitals. *The Journal of Chemical Physics* **1985**, *83*, 1736–1740.

(41) Reed, A. E.; Weinstock, R. B.; Weinhold, F. Natural population analysis. *The Journal of Chemical Physics* **1985**, *83*, 735–746.

(42) Carpenter, J. E.; Weinhold, F. Analysis of the geometry of the hydroxymethyl radical by the "different hybrids for different spins" natural bond orbital procedure. *Journal of Molecular Structure: THEOCHEM* **1988**, *169*, 41–62.

(43) Reed, A. E.; Curtiss, L. A.; Weinhold, F. Intermolecular interactions from a natural bond orbital, donor-acceptor viewpoint. *Chemical Reviews* **1988**, *88*, 899–926.

(44) Weinhold, F.; Carpenter, J. E. In *The Structure of Small Molecules and Ions*; Naaman, R., Vager, Z., Eds.; Springer US: Boston, MA, 1988; pp 227–236.

(45) Zhao, Y.; Truhlar, D. G. The M06 suite of density functionals for main group thermochemistry, thermochemical kinetics, noncovalent interactions, excited states, and transition elements: two new functionals and systematic testing of four M06-class functionals and 12 other functionals. *Theoretical Chemistry Accounts* **2008**, *120*, 215–241.

(46) Dunning, T. H., Jr. Gaussian basis sets for use in correlated molecular calculations. I. The atoms boron through neon and hydrogen. *The Journal of Chemical Physics* **1989**, *90*, 1007–1023.

(47) Kendall, R. A.; Dunning, T. H.; Harrison, R. J. Electron affinities of the first-row atoms revisited. Systematic basis sets and wave functions. *The Journal of Chemical Physics* **1992**, *96*, 6796–6806.

(48) Woon, D. E.; Dunning, T. H. Gaussian basis sets for use in correlated molecular calculations. III. The atoms aluminum through argon. *The Journal of Chemical Physics* **1993**, *98*, 1358–1371.

(49) Peterson, K. A.; Figgen, D.; Goll, E.; Stoll, H.; Dolg, M. Systematically convergent basis sets with relativistic pseudopotentials. II. Small-core pseudopotentials and correlation

consistent basis sets for the post-d group 16–18 elements. *The Journal of Chemical Physics* **2003**, *119*, 11113–11123.

(50) Peterson, K. A.; Shepler, B. C.; Figgen, D.; Stoll, H. On the Spectroscopic and Thermochemical Properties of ClO, BrO, IO, and Their Anions. *The Journal of Physical Chemistry A* **2006**, *110*, 13877–13883.

(51) Kozuch, S.; Martin, J. M. L. Halogen Bonds: Benchmarks and Theoretical Analysis. *Journal of Chemical Theory and Computation* **2013**, *9*, 1918–1931.

(52) Boys, S.; Bernardi, F. The calculation of small molecular interactions by the differences of separate total energies. Some procedures with reduced errors. *Molecular Physics* **1970**, *19*, 553–566.

(53) Badger, R. M. A Relation Between Internuclear Distances and Bond Force Constants. *The Journal of Chemical Physics* **1934**, *2*, 128–131.

(54) Kraka, E.; Zou, W.; Tao, Y. Decoding chemical information from vibrational spectroscopy data: Local vibrational mode theory. *WIREs Computational Molecular Science* **2020**, *10*, e1480.

(55) Rahm, M.; Hoffmann, R.; Ashcroft, N. W. Atomic and Ionic Radii of Elements 1–96. *Chemistry – A European Journal* **2016**, *22*, 14625–14632.

(56) Frisch, M. J.; Trucks, G. W.; Schlegel, H. B.; Scuseria, G. E.; Robb, M. A.; Cheeseman, J. R.; Scalmani, G.; Barone, V.; Petersson, G. A.; Nakatsuji, H. et al. Gaussian 16 Revision C.01. 2016.

(57) Lu, T.; Chen, F. Multiwfn: A multifunctional wavefunction analyzer. *Journal of Computational Chemistry* **2012**, *33*, 580–592.

(58) Bader, R. F. W. Bond Paths Are Not Chemical Bonds. *The Journal of Physical Chemistry A* **2009**, *113*, 10391–10396.

(59) Bader, R. F. W.; Carroll, M. T.; Cheeseman, J. R.; Chang, C. Properties of atoms in molecules: atomic volumes. *Journal of the American Chemical Society* **1987**, *109*, 7968–7979.

(60) Bader, R. F. W.; Nguyen-Dang, T. T. In *Advances in Quantum Chemistry*; Löwdin, P.-O., Ed.; Academic Press, 1981; Vol. 14; pp 63–124.

(61) Stone, J. *An Efficient Library for Parallel Ray Tracing and Animation*. M.Sc. thesis, Computer Science Department, University of Missouri-Rolla, 1998.

(62) Humphrey, W.; Dalke, A.; Schulten, K. VMD: Visual molecular dynamics. *Journal of Molecular Graphics* **1996**, *14*, 33–38.

(63) Kraka, E.; Cremer, D. Dieter Cremer's contribution to the field of theoretical chemistry. *International Journal of Quantum Chemistry* **2019**, *119*, e25849.

(64) Tao, Y.; Zou, W.; Nanayakkara, S.; Kraka, E. LModeA-nano: A PyMOL Plugin for Calculating Bond Strength in Solids, Surfaces, and Molecules via Local Vibrational Mode Analysis. *Journal of Chemical Theory and Computation* **2022**, *18*, 1821–1837.

(65) Zou, W.; Tao, Y.; Freindorf, M.; Makos, M.; Verma, N.; Kraka, E. LMODEA; Computational and Theoretical Chemistry Group (CATCO), SMU: Dallas, TX, 2022.

(66) pandas development team, T.; pandas-dev/pandas: Pandas, version 1.4.4; Zenodo 2020, `https://doi.org/10.5281/zenodo.3509134` (accessed February 2023).

(67) Wes McKinney, Data Structures for Statistical Computing in Python. Proceedings of the 9th Python in Science Conference. 2010; pp 56 – 61.

(68) Waskom, M. L. seaborn: statistical data visualization. *Journal of Open Source Software* **2021**, *6*, 3021.

(69) Hunter, J. D. Matplotlib: A 2D Graphics Environment. *Computing in Science Engineering* **2007**, *9*, 90–95.

(70) Delgado, A. A. A.; Humason, A.; Kalescky, R.; Freindorf, M.; Kraka, E. Exceptionally Long Covalent CC Bonds—A Local Vibrational Mode Study. *Molecules* **2021**, *26*, 950.

(71) Decato, D. A.; Sun, J.; Boller, M. R.; Berryman, O. B. Pushing the limits of the hydrogen bond enhanced halogen bond—the case of the C–H hydrogen bond. *Chemical Science* **2022**, *13*, 11156–11162.

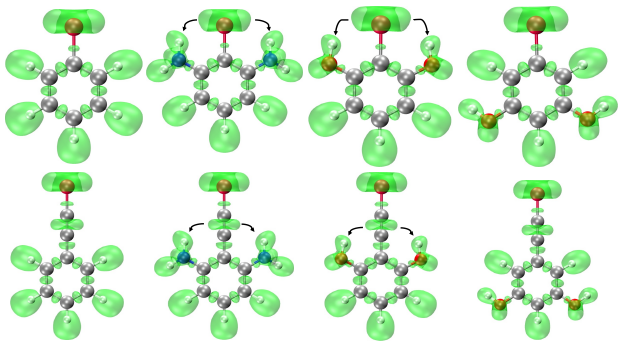

Table of Contents Only